HHS Public Access

Author manuscript

ACS Nano. Author manuscript; available in PMC 2024 August 22.

Published in final edited form as:

ACS Nano. 2023 August 22; 17(16): 15542–15555. doi:10.1021/acsnano.3c02013.

Neutrophil-Mediated Delivery of Nanocrystal Drugs via Photoinduced Inflammation Enhances Cancer Therapy

Yujie Su,

Department of Pharmaceutical Sciences, College of Pharmacy and Pharmaceutical Sciences, Washington State University, Spokane, Washington 99202, United States

Jin Gao,

Department of Pharmaceutical Sciences, College of Pharmacy and Pharmaceutical Sciences, Washington State University, Spokane, Washington 99202, United States

Xinyue Dong,

Department of Pharmaceutical Sciences, College of Pharmacy and Pharmaceutical Sciences, Washington State University, Spokane, Washington 99202, United States

Kraig A. Wheeler,

Department of Chemistry, Whitworth, University, Spokane, Washington 99251, United States

Zhenjia Wang

Department of Pharmaceutical Sciences, College of Pharmacy and Pharmaceutical Sciences, Washington State University, Spokane, Washington 99202, United States

Abstract

*Corresponding Author: Zhenjia Wang – Department of Pharmaceutical Sciences, College of Pharmacy and Pharmaceutical Sciences, Washington State University, Spokane, Washington 99202, United States; zhenjia.wang@wsu.edu.

Author Contributions

Y.S. and Z.W. conceived and designed the experiments. Y.S., J.G., and X.D. performed the experiments. Y.S., J.G., and Z.W analyzed and discussed the results. K.A.W. performed the X-ray measurement of paclitaxel nanocrystals. Y.S. and Z.W. wrote the manuscript. Z.W. supervised the projects related to neutrophil-based drug delivery.

The authors declare no competing financial interest.

ASSOCIATED CONTENT

Supporting Information

The Supporting Information is available free of charge at https://pubs.acs.org/doi/10.1021/acsnano.3c02013.

Tables S1–S4 show the particle sizes, Zeta potential, and PDI of different NPs; Figures S1–S25 show the resolution of acute inflammation after laser irradiation; CD11b expression levels on leukocytes without laser irradiation; CD11b expression levels on leukocytes in blood; Anit-CD11b coating on gold NPs; CD11b expression levels on HL-60 cells; Uptake of gold NPs by HL-60 cells; Depletion of neutrophils *in vivo*; Tumor delivery efficiency of gold NPs; SEM images of PTX NC and PEG/PTX NC; X-ray diffraction pattern of PEG/PTX NC; Uptake of PTX NC by HL-60 cells; Neutrophil-mediated delivery of PTX NC in inflamed lung; Intravital images of tumor vessels; Uptake of Ab/ PTX NC by leukocytes; Flow cytometry graph of PTX NC positive neutrophils; Delivery efficiencies of PTX in liver, spleen, and tumor; Cell viability of 3LL cells; Apoptosis of differentiated HL-60 cells; HPLC of PTX released from differentiated HL-60 cells; HPLC of PTX release from liposomes; Individual 3LL tumor growth curves; H&E staining images of major organs; Individual GL261 tumor growth curves; Neutrophil-mediated delivery of Ab/PTX LP for tumor therapy; PTX loading efficiency in neutrophils (PDF)

Video S1 shows that neutrophils (violet) take up Ab/PTX NCs (green) in blood and most neutrophils adhered to vessel walls, and some neutrophils have migrated across tumor blood vessels (full caption in SI PDF) (MP4)

Video S2 and Video S3 show that neutrophils (violet) carrying Ab/PTX NCs (green) accumulate outside tumorous vasculature (full caption in SI PDF) (MP4) (MP4)

Complete contact information is available at: https://pubs.acs.org/10.1021/acsnano.3c02013

The efficient delivery of anticancer agents into tumor microenvironments is critical for the success of cancer therapies, but it is a prerequisite that drug carriers should overcome tumor vasculature and possess high drug contents. Here, we found that photoinduced inflammation response caused the migration of neutrophils into tumor microenvironments and neutrophils transported neutrophil-targeted nanoparticles (NPs) across the tumor blood barrier. The results showed that tumor delivery efficiencies of NPs were 5% ID/g, and they were independent of particle sizes (30–200 nm) and their doses (10^8–10^{11} NPs). To efficiently deliver anticancer agents into tumors via neutrophils, we fabricated carrier-free paclitaxel nanocrystals (PTX NC). The results showed that neutrophil uptake of PTX NC did not impair neutrophil tumor infiltration, and the sustainable release of PTX from PTX NC in tumors was regulated by paclitaxel protein complexes, thus improving the mouse survival in two preclinical models. Our studies demonstrate that delivery of nanocrystal drugs via neutrophils is a promising method to effectively treat a wide range of cancers, and we have also identified a mechanism of drug release from neutrophils in tumors.

Graphical Abstract

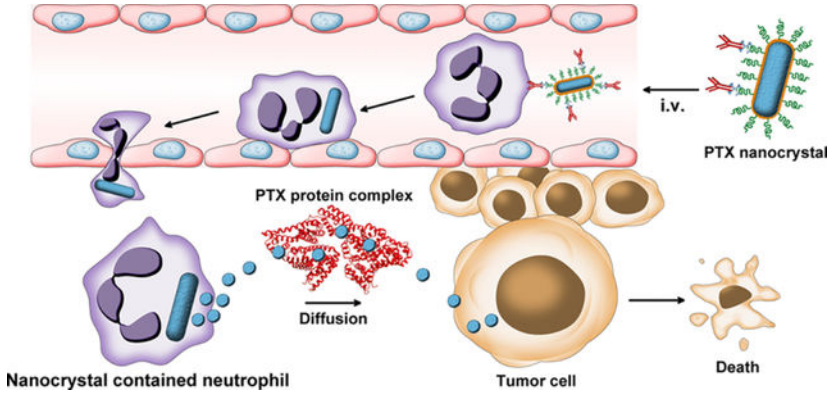

Keywords

neutrophil-mediated drug delivery; tumor delivery efficiency; particle size/dose; paclitaxel nanocrystals; drug protein complexes; protein-enhanced drug release; carrier-free drug NPs

The efficient delivery of anticancer agents into tumor microenvironments is essential to successfully treat cancers. To achieve this goal, nanoparticles (NPs) have been exploited to deliver anticancer agents into tumor microenvironments based on the enhanced permeability and retention (EPR)[1–3] effect. However, three decades of nanomedicine research and development have shown its limited clinical translation in cancer treatments.[4–6] There are several reasons. For example, there is a high interstitial pressure in tumor microenvironments to prevent the accumulation of NPs in tumors.[7] The tumor vasculature is heterogeneous and dependent on cancer types, their stages, and patient populations, therefore it is hard to predict the EPR effect in all tumors.[8,9] The recent meta-analysis on cancer nanomedicine research in the past 10 years has shown that nanoparticle delivery to solid tumors was 0.7% (a median value) of injected dose,[10] and the experimental studies show that the delivery of NPs to cancer cells was 0.0014% of injected dose.[11] Furthermore, recent studies[12] demonstrate that there are few endothelial gaps on tumor vasculature

and more than 90% of NPs enter tumors through the endothelium. Compelling studies and data indicate that tumor vasculature is a physical barrier to prevent the delivery of nanotherapeutics into tumors.

Inflammation is the immune response to infections or tissue injury.[13] This process is involved with leukocyte infiltration across blood vasculature.[14–16] Neutrophils are the most abundant leukocytes (50–75% in humans) and represent the first line of defense in response to inflammation that is associated with neutrophil transmigration across the blood barrier.[17] *In situ* nanoparticle targeting of circulating neutrophils could deliver NPs across tumor vasculature.[18] The studies are focused on delivery of nontoxic agents via neutrophils, such as gold NPs and a photosensitizer.[19–21] Although some studies delivered toxic agents using neutrophils for cancer therapies including either attaching of drug NPs to the surface of neutrophils[22] or uptake of drug NPs in neutrophils,[23] it remains unknown whether drug NPs impair neutrophil tumor tropism and how efficiently neutrophils deliver drug NPs. Neutrophils are potential carriers to overcome tumor vasculature; however, it is required that drug carriers should possess high drug content because neutrophils have a limited volume to lodge many drug carriers per cell. It is necessary to address these fundamental questions in neutrophil-mediated drug delivery.

Cancer nanomedicines are focused on engineering a wide range of NPs with different sizes and targeting ligands,[24–26] and smaller NPs are used to enhance tumor targeted delivery.[25,27–31] Most drug carriers possess less than 10% of an active drug, so administration of a large amount of carrier materials is needed to achieve a clinically relevant dose of a drug, resulting in the undesirable side effects of carrier materials.[32] Nanocrystal drugs are made of self-assembled drugs without carrier excipients and with nearly 100% drug loading efficiency; thus, nanocrystal drugs can be administered at a very low number of particles. Nanocrystal drugs have been used in clinics to treat infectious diseases and immune diseases because of their long acting therapy, high drug loading, easy clinical manufacture, and low production cost.[33]

Here, we designed paclitaxel nanocrystals (PTX NC) coated with anti-CD11b antibody (Ab) (Ab/PTX NC) that can specifically target activated neutrophils, and neutrophils take up and transport Ab/PTX NC across tumor vasculature. To assess the neutrophil-mediated delivery efficiency of NPs, we utilized gold NPs because we can precisely measure gold NPs in tumor tissues. We found that neutrophil-mediated delivery of NPs into tumors was independent of particle sizes (30–200 nm in diameter) and their doses (10^8–10^{11} NPs) and the tumor delivery efficiency was 5% ID/g. When we studied the tumor delivery of Ab/PTX NC, using intravital microscopy, we observed that neutrophils efficiently took up Ab/PTX NC in blood and transported Ab/PTX NC across tumor vasculature. The flow cytometry and confocal microscopy showed that the uptake of Ab/PTX NC did not inhibit neutrophil transmigration into tumor tissues. We identified a molecular mechanism in which Ab/PTX NC in neutrophils sustainably released PTX, and subsequently, PTX permeabilized the cell membrane and formed a PTX-protein complex for the killing of tumor cells in tumor microenvironments. Interestingly, we observed that the high drug loading of NPs is essential for neutrophil-mediated drug delivery to treat cancer compared to the low drug loading of liposomes. Figure 1 is the design of Ab/PTX NC for targeting activated neutrophils, the

hypothesis that Ab/PTX NC are delivered into tumor tissues through a neutrophil-mediated pathway, and the mechanism of PTX release from Ab/PTX NCs in neutrophils.

RESULTS AND DISCUSSION

Acute Inflammation Induces Neutrophil Tumor Infiltration.

To generate neutrophil migration into tumor microenvironments, we created an acute inflammation in tumor tissues via photosensitization.[20,34] 3LL tumor was chosen as it is a standard preclinical solid tumor model in laboratories[35] and maintains tumor blood barriers.[36,37] In the experiments, 3LL mouse tumor tissues were exposed to a laser at 650 nm 45 min after intravenous (i.v.) injection of pyropheophorbide-a (Ppa) to tumor bearing mice. Ppa was a photosensitizer that increased local inflammatory signals after it absorbed the light.[20] First, we measured inflammatory signals in tumor tissues after laser irradiation and observed that IL-6 and TNF-α temporally increased after laser irradiation (Figure 2a, b). Similarly, cytokines IL-6 and TNF-α significantly increased in blood at 6 h after the laser irradiation and reached the maximum value at 12 h (Figure. 2c, d). Furthermore, we measured neutrophil percentages in blood and tumor tissues after laser irradiation to tumors. It was shown that neutrophils rapidly rose in blood after laser irradiation and reached a peak at 12 h, in which neutrophils increased by 10-fold compared to those without laser irradiation (Figure 2e, f). Concurrently, we found that neutrophils in tumor tissues continuously increased from 5% at 0 h to 18% at 24 h (Figure 2g, h), revealing a quick neutrophil migration from blood into tumor tissues. The results indicate that laser irradiation induces an acute inflammatory response in tumor microenvironments to attract neutrophils from blood to tumor tissues; therefore neutrophils could be transporters to deliver therapeutics across blood vessels if NPs can specifically target these neutrophils. To verify that the photoinduced inflammation response was an acute process, we measured blood neutrophils in the mice. We found that neutrophils dropped to the basal level 48 h after laser irradiation (Figure S1), indicating that the photoinduced inflammation is acute and can be resolved. Therefore, laser irradiation may not affect mouse homeostasis in long-term studies in cancer therapies.

Tumor Delivery Efficiencies of NPs via Neutrophil-Mediated Pathway.

Specifically targeting activated neutrophils *in situ* is a critical step to deliver NPs into tumors via a neutrophil-mediated pathway. CD11b is a membrane protein highly expressed on activated neutrophils and is upregulated during acute inflammation.[20,38] Importantly, human neutrophils also increase the expression of CD11b in the inflammation response,[39,40] therefore there is the potential for clinical translation if we specifically target activated neutrophils via CD11b. We first addressed whether CD11b was highly expressed on activated neutrophils compared to that on other types of leukocytes in blood after tumor laser irradiation. Without laser exposure to tumors, CD11b expression levels on neutrophils were 4 times higher than those on monocytes (Figure S2, S3). In addition, laser irradiation to the tumors increased the expression of CD11b on activated neutrophils by 8-fold compared to that on monocytes and 160-fold compared to other types of leukocytes (Figure 3a and Figure S3). Furthermore, after laser exposure to tumors, the number of neutrophils was 4 times higher than that of monocytes in the blood (Figure S3). The results indicate that

neutrophils dominated in blood after laser priming of tumors and upregulated CD11b on neutrophils compared to other leukocytes including monocytes. Therefore, CD11b is a target to design NPs that specifically target activated neutrophils.

We conjugated Ab to gold NPs (Ab-Au), thus gold NPs selectively bound to activated neutrophils in blood and subsequently were internalized. Since gold NPs are inert *in vivo*,[41–43] we can accurately measure nanoparticle delivery efficiencies via neutrophils into tumor tissues. Gold NPs were coated by PEG (PEG-Au) as the control for neutrophil targeting and PEG coating can also reduce nanoparticle opsonization.[44,45] In the experiments, Ab-Au NPs or PEG-Au NPs were prepared through the binding of biotin-Ab or biotin-PEG to neutravidin functionalized on spherical gold NPs (Figure 3b). We prepared two sizes of gold NPs (30 and 200 nm) and two types of coating (PEG and Ab). Their hydrodynamic diameters, zeta potentials and polydispersity indices were measured (Table S1). The data showed that the coating of PEG or Ab did not change the surface charges of NPs and their sizes, suggesting that PEG-Au and Ab-Au have similar physical properties. The coating of Ab on gold NPs was quantified by SDS-PAGE analysis, and it was shown that there were 19.7 and 3.1 μg of Ab per mg of gold 30 and 200 nm NPs (Figure 3c and Figure S4), respectively. When we calculated the surface areas of gold NPs, we found that there was similar density of Ab on 30 and 200 nm gold NPs. Next, we performed cellular uptake of NPs using HL-60 cells because they showed neutrophil-like functions.[46,47] We found that CD11b was highly expressed on HL-60 cells, and it was upregulated after HL-60 cells were differentiated (Figure S5) consistent with the previous results.[47] The studies on the uptake of gold NPs in differentiated HL-60 cells showed that Ab coating to NPs increased the cellular uptake of NPs compared to PEG-coated NPs, suggesting that CD11b on the cell surface promoted the uptake of NPs (Figure S6).

Neutrophil-mediated delivery efficiencies of gold NPs into tumors were measured in a 3LL subcutaneous tumor mouse model. The inflammation was generated in tumor tissues by laser. Three h after laser irradiation, 30 nm Ab-Au NPs at 1.2 mg/kg or 200 nm Ab-Au NPs at 6 mg/kg were i.v. injected into mice via a tail vein. At these doses, 30 nm-sized NPs had the similar surface areas to 200 nm-sized NPs, thus both NPs possessed the similar number of Ab. Twenty-four h after administration of NPs, we collected tumor tissues and quantified the percentages of administered NPs in tumors (Figure 3d, e). Without laser exposure, tumor delivery efficiencies did not depend on the coating of either PEG or Ab. However, laser exposure to tumor tissues dramatically increased the delivery efficiencies of Ab-Au NPs for both sizes of NPs, indicating that an increased tumor delivery of NPs was associated with laser irradiation. Furthermore, when we depleted neutrophils using anti-Ly6G antibody (Figure S7), we observed that Ab-coated NPs were dramatically decreased in tumors, and tumor uptake of NPs was similar to that without laser tumor irradiation. This indicated that neutrophils played a central role in the delivery of NPs into tumors. It was also observed that Ab coating to NPs was the prerequisite for increased tumor delivery when we compared them to PEG-coated NPs (Figure 3d, e). Finally, we isolated neutrophils from inflamed tumor tissues 24 h after administration of gold NPs, and then, we quantitatively measured NPs in neutrophils using inductively coupled plasma mass spectrometry (ICP-MS). We found that neutrophils took up similar amounts of administered NPs for both sizes of NPs (Figure 3f), indicating that neutrophil uptake of NPs was not dependent on NP size.

Together, the data show that NPs can *in situ* selectively target activated neutrophils, and subsequently, neutrophils mediate the delivery of NPs into tumor microenvironments.

Furthermore, we studied whether the size and dose of NPs affected neutrophil-mediated tumor delivery. We measured tumor delivery efficiencies of NPs with or without laser priming of tumor tissues in a wide range of doses (10^8–10^{12} of NPs) (Figure S8). We observed that laser irradiation of tumors increased tumor delivery of NPs. The increased tumor delivery was associated with the neutrophil-mediated pathway; therefore, we subtracted the delivery efficiencies of the NPs without laser exposure to tumors. The results (Figure 3g) showed that neutrophil-mediated delivery of NPs into tumors was independent of the particle sizes (30–200 nm) and doses (10^8 to 10^{11}). Interestingly, increased numbers of NPs beyond 10^{12} (such as 30 nm NPs at 30 mg/kg) decreased the tumor delivery efficiency by neutrophils, which may be related to the saturation of neutrophil nanoparticle uptake due to the limited cell volume.

Neutrophils Deliver PTX NC Across Tumor Vasculature.

Neutrophil-mediated drug delivery in tumors requires that drug carriers have a high drug loading because of a limited cell volume to house drug carriers. Small molecule drugs are self-assembled to form nanocrystals that are carriers free with almost 100% drug loading and nanocrystal drug formulations possess the sustainable and slow release of a drug.[48] Here, we hypothesized that neutrophils transported nanocrystal drugs across the tumor vasculature to increase the tumor delivery of drugs.

We used a high-pressure homogenization method to produce PTX NC. During the high-pressure homogenization, we coated nanocrystals with mPEG-DSPE and biotin-PEG-DSPE for the bioconjugation of Ab to the nanoparticle surface. The SEM images (Figure S9) showed a rod-like nanostructure of PTX NC and PEG-coated PTX NC (PEG/PTX NC). We measured the X-ray diffraction of PEG/PTX NC powders, and the X-ray spectrum exhibited the crystalline structures of the PTX NC (Figure S10). The measurement is consistent with the previous studies.[49] Figure 4a shows the morphology of the PTX NC coated with Ab (Ab/PTX NC). The Ab/PTX NCs showed homogeneous rodlike structures with 350 nm diameter determined by dynamic light scattering, and the sizes were increased compared to the nanocrystals coated with PEG or bare nanocrystals (Table S2). The size increase was associated with the coating of Ab, consistent with the SDS-PAGE result showing that Ab was successfully coated to nanocrystals (Figure 4b). We evaluated the targeting ability of Ab/PTX NCs for differentiated HL-60 cells. The studies on *in vitro* uptake of nanocrystals showed that cellular uptake of Ab/PTX NC was 3 folds higher than that of PEG/PTX NC (Figure S11), suggesting that CD11b on HL60 cells promoted nanocrystal uptake.

As PTX is a cytotoxic drug, PTX NC may impair neutrophil trafficking after neutrophils take up nanocrystals. We employed an acute lung inflammation model to investigate whether the uptake of PTX NC mitigated neutrophil transmigration *in vivo*. In acute lung inflammation, intratracheal administration of lipopolysaccharide (LPS) causes neutrophil transmigration from blood to the airspace of the lung.[50,51] This process allows us to quantitatively analyze neutrophil-mediated delivery of NPs across the blood vessel barrier *in vivo*. We collected neutrophils in bronchoalveolar lavage (BAL) after we administered

PTX NC, and then we imaged them using confocal microscope. It was clear to observe the fluorescence of Ab/PTX NCs in neutrophils compared to that of PEG/PTX NC (Figure S12a). Flow cytometry analysis showed that 42% of infiltrated neutrophils contained Ab/PTX NC. In contrast, there was less than 11% infiltrated neutrophils containing PEG/PTX NC (Figure S12b, d). The results indicated that coating of Ab to NPs increased the neutrophil targeting, and neutrophils transported PTX NC across the blood vessel barrier *in vivo*. Furthermore, we measured the total of neutrophils in the lung lavage, and we observed that the total neutrophils were independent of the coating of Ab or PEG to nanocrystals (Figure S12c, e). This showed that even though neutrophils carried PTX NC, the neutrophils still migrated from blood to the airspace in the lung. Together, the results show that neutrophil uptake of PTX NC does not inhibit neutrophil trafficking. This allows us to investigate the delivery of PTX NC into tumor microenvironments via neutrophils.

First, we visualized neutrophil transport of PTX NC in tumor microenvironments in real-time using intravital microscopy. In the experiments, 45 min after 3LL subcutaneous tumor was exposed to laser, FITC-labeled PEG/PTX NC or Ab/PTX NC was i.v. administered. Thirty minutes later, Alexa fluor 647-labeled antimouse Ly6G antibody was i.v. injected to mark neutrophils. One h later, Cy3-BSA was injected to visualize the blood vessels. After tumor tissues were exposed to the laser, it was observed that neutrophils transmigrated into tumor parenchyma (Figure S13). When Ab/PTX NC were i.v. administered, it was shown that the nanocrystals colocalized with infiltrated neutrophils in the extravascular space (Figure 4c). However, most PEG/PTX NC were found in intravascular areas when they were administered to mice, and neutrophils did not take up nanocrystals (Figure 4c). The real-time 3D intravital microscopic imaging showed that Ab/PTX NC laden neutrophils adhered to the vessel walls (Supplementary Video S1), transmigrated across the vascular walls, and formed a cluster of neutrophils (Supplementary Video S2). We also observed that neutrophils carrying PTX NC were moving in tumor tissues (Supplementary Video S3). The intravital microscopy demonstrated that neutrophils took up Ab/PTX NC in blood and transported them into tumor microenvironments.

We further validated whether neutrophils were dominant in mediating the delivery of Ab/PTX NC. We analyzed the flow cytometry data of circulating leukocytes and their uptake of nanocrystals under or without laser irradiation (Figure S14). The uptake efficiencies of nanocrystals were calculated by the mean fluorescence intensities of nanocrystals multiplied with the leukocyte percentages, and then they were normalized relative to monocyte uptake of nanocrystals. The results (Figure 4d) showed that laser irradiation increased neutrophil uptake of nanocrystals compared with monocytes and other leukocytes, and the neutrophil uptake efficiency of nanocrystals was more than 13 times higher than other circulating leukocytes when the tumor was exposed to the laser. The data clearly indicate that neutrophils are major cells in circulation to take up nanocrystals after laser exposure to tumors, consistent with our observation by using intravital microscopy (Figure 4c).

We next quantitatively studied the neutrophil transport of PTX NC into tumor microenvironments. FITC-labeled PEG/PTX NC or Ab/PTX NC was i.v. administered to 3LL tumor mice 3 h after laser irradiation to tumors. Neutrophils in tumor tissues were isolated 6 h after administration of nanocrystals, and confocal imaging showed that

most neutrophils contained nanocrystals when Ab was coated to nanocrystals, but few neutrophils possessed PEG-coated nanocrystals (Figure 4e). The results are consistent with the observation using intravital microscopy, indicating that neutrophils transport nanocrystals into the tumor microenvironments.

Furthermore, neutrophils were isolated from tumor tissues 24 h after administration of nanocrystals, and neutrophil uptake of nanocrystals and their trafficking were analyzed by using flow cytometry. Without laser exposure to tumors, there were less than 2% tumor neutrophils containing PEG/PTX NC or Ab/PTX NC. However, 7.7% tumor neutrophils contained Ab/PTX NC after laser exposure to the tumors. When PEG-coated nanocrystals were administered, there were only 3.5% neutrophils containing nanocrystals that were comparable to the neutrophil uptake of nanocrystals without laser exposure to tumors (Figure 4f and Figure S15). The results showed neutrophil-mediated transport of nanocrystals into the tumor via light-induced acute inflammation. Next, we measured total neutrophils in tumor tissues (Figure 4g). Without the laser exposure to tumors, we observed around 7% neutrophils in tumors, and the percentages were independent of administration of PEG-coated or Ab-coated nanocrystals. However, when the laser was exposed to the tumors, neutrophil percentages increased by 2–3 times compared to those in the case of without laser irradiation. This increase was associated with neutrophil tumor infiltration. Interestingly, the number of neutrophils in tumors was independent of administered nanocrystals, indicating that neutrophil uptake of NPs did not impair neutrophil tumor infiltration. Together, the data clearly show that neutrophils mediate the delivery of PTX NC to tumor microenvironments, and uptake of NPs does not inhibit neutrophil transmigration.

We also measured the dynamics of the biodistribution of PTX NC (Figure S16). While liver and spleen took up most administered nanocrystals, we observed that laser exposure to tumors enhanced the delivery efficiency of PTX NC in tumors. It was shown that the area under the curve (AUC) of PTX in tumors mediated by the neutrophil pathway was 2.4 times higher than that of conventional delivery (Figure 4h). The data are consistent with delivery of gold NPs as shown in Figure 2.

Dissolution of PTX NC Is Regulated by a PTX-Protein Complex for Sustainable Drug Release to Kill Tumor Cells.

It is not clear how PTX NC is released from neutrophils to kill cancer cells in tumor microenvironments. We first studied the drug release and cytotoxicity of PTX NC *in vitro*. The PTX release was determined using a dialysis method against a PBS buffer (pH 7.4). The PTX release profile from PEG/PTX NC or Ab/PTX NC was similar, and the release sustained for 48 h (Figure 5a) consistent with the dissolution process of nanocrystal drugs.[52] Ab/PTX NC were incubated with 3LL cells for 24 or 48 h, respectively, and the cell viability was quantified by MTT assay (Figure 5b). PTX NC were able to kill tumor cells, and cellular killing was dependent on incubation time, implying that PTX NC sustainably released free PTX to kill cancer cells, consistent with their release profile (Figure 5a).

To address how PTX NC in neutrophils was released to kill tumor cells, we designed *in vitro* experiments as shown in Figure 5c. In the experiment, Ab/PTX NC were incubated with differentiated HL-60 cells for 1 h, and then the cells were purified and were

subsequently lysed. The HPLC results showed that PTX in the cell lysate was 16 μg of PTX per 10^6 HL-60 cells, indicating that HL60 cells took up nanocrystals. Next, a series of concentrations of Ab/PTX NC-laden cells were cultured in fresh media for 24 or 48 h, and then the culture media were collected and subsequently incubated with tumor cells to measure cell viability (Figure 5d). In the control, the same experiment as shown in Figure 5c was performed at the same number of HL-60 cells without PTX NC. We found that the culture media of HL-60 cells alone did not affect the cell viability of 3LL tumor cells (Figure S17). However, the culture media of HL-60 cells containing Ab/PTX NC killed tumor cells (Figure 5d), and the cell viability was strongly dependent on the PTX amounts loaded inside HL-60 cells and the incubation time. The results indicated that the culture media contained PTX to kill tumor cells, but it is unclear how PTX NC released from cells.

We hypothesized that HL-60 cells may die via the apoptosis pathway to release PTX NC. We measured the cell apoptosis, but we did not observe that many cells died within 24 h (Figure S18). To further address the release of PTX NC from cells, the cells were cultured for 24 h in a fresh medium after the cells took up PTX NC. Then we removed the cells to obtain the culture media. We centrifuged the media again to acquire the supernatant and pellet. We measured particle sizes in the supernatant and pellet using dynamic light scattering. We observed 17 nm particles in the supernatant and 345 nm particles in the pellet (Table S3). The HPLC studies showed that the supernatant contained PTX. We hypothesized that 17 nm-sized particles in the supernatant may be associated with the binding of PTX to proteins because there is the high protein binding affinity of PTX.[53] To address this question, we employed a 30 kDa filter to separate free PTX and PTX-protein complexes in the supernatant and quantified them using HPLC (Figure S19a). We found that the majority of PTX was in the form of PTX-protein complexes in the supernatant. To further confirm PTX-protein complexes, we incubated PTX NC with BSA or mouse serum, collected the supernatant, and measured free PTX and PTX-protein complexes after the supernatant was centrifuged using a 30 kDa filter. The results were similar to the data in (Figure S19a), showing that PTX formed the protein complexes. We also observed PTX in the pellet obtained from the culture medium (Figure S19b). Next, we measured the time course of the PTX contents in the supernatant (Figure 5e) and the pellet (Figure 5f) of culture media. The results showed that it is unlikely that PTX nanocrystals were directly released from cells. However, most PTX was in the form of PTX-protein complexes, suggesting that PTX was dissolved from PTX NC in the cells, crossed cell membrane, and subsequently formed PTX-protein complexes in culture media.

However, it is unclear how PTX-protein complexes crossed the cell membrane after its dissolution from PTX NC. To address this question, we loaded PTX/BSA complexes inside liposomes (PTX/BSA LP) and measured how PTX released from the liposomes (Figure 5g). This was designed to simulate the PTX release from cells. PTX/BSA LP was suspended in PBS, and then we collected the supernatant after we centrifuged the liposome suspension. We measured the supernatant and observed a small signal of PTX (Figure S20a). However, when the PTX/BSA LP was suspended in a buffer containing BSA, the PTX signal dramatically increased (Figure S20b), and the majority of PTX was in the form of PTX-protein complexes. Furthermore, we studied the dynamics of PTX release from PTX/BSA LP in PBS (Figure 5h) and PBS containing BSA (Figure 5i). We

observed that there was limited release of PTX in 24 h when PTX/BSA LP was dispersed in PBS. However, the PTX release was temporally increased when PTX/BSA LP was dispersed in a buffer containing BSA. The increase of PTX release may be associated with increased diffusion rate of PTX from liposomes because BSA increased the solubility of PTX compared to that in PBS. Together, we demonstrated a molecular mechanism by which PTX was released from PTX NC in the cells. The process enabled the sustainable release of PTX after neutrophils delivered PTX NC in tumor microenvironments.

Neutrophil-Mediated Delivery of PTX NC Improves Mouse Survival in Cancer Models.

We next addressed whether neutrophil-mediated delivery of PTX NC enhanced cancer therapies in mouse models. In the mouse lung cancer model, mice were injected with Ppa, and 1 h later, the mouse tumor was exposed to the laser at 650 nm. Different drug formulations containing the same 5 mg/kg PTX were i.v. administered 3 h after laser exposure to the tumor, and the second dose was administered on Day 6 following the same procedure. It was observed that Ab/PTX NC or laser irradiation alone did not inhibit the tumor growth (Figure 6a and Figure S21) compared to the control (PBS treatment). However, the combination therapy of Ab/PTX NC and laser irradiation significantly delayed the tumor growth and dramatically prolonged the mouse survival compared to all controls (Figure 6b). During the experiments, we monitored mouse behaviors and measured mouse body weights (Figure 6c). We did not observe the weight loss of mice and their health issues. We also performed the H&E staining of the major organs after the treatment (Figure S22). There were no noticeable histological changes, indicating that mice were tolerable to the combinatory therapy of PTX NC and laser irradiation. Furthermore, we tested PTX NC in a glioma mouse model following the same procedure as in Figure 6a–c. Glioma is a malignant solid tumor showing a tight tumor vascular barrier,[54–56] thus it is the good model to further test our hypothesis on neutrophil-mediated drug delivery. The results showed that delivery of PTX NC via neutrophil pathway delayed the tumor growth (Figure 6d and Figure S23), increased the mouse survival (Figure 6e) and did not change the mouse weight (Figure 6f). The tumor inhibition in the glioma model was less efficient than in the 3LL model, which may be associated with the efficacy of PTX depending on cancer types.

The current nanoparticle-based drug carriers have the drug loading at less than 10% (w/w).[57] It is not known whether the neutrophil-mediated delivery pathway is useful for this type of drug carrier. We first prepared PTX-loaded liposomes and functionalized them with Ab (Ab/PTX LP). The PTX loading efficiency is 2.5% in liposomes. The particle sizes and Zeta potentials of Ab/PTX LP were about 200 nm in diameter and −9.7 mV, respectively (Table S4). We labeled liposomes with a 3,3′-dioctadecyloxacarbocyanine perchlorate (DIO) fluorescent dye, and the liposomes were i.v. administered to 3LL tumor mice following the protocol as shown in Figure S24a. After we collected tumor tissues, we analyzed neutrophils using flow cytometry. It was shown that neutrophils were significantly increased after laser irradiation of tumors (Figure S24b), which was consistent with the data as shown in Figure 2h. We also observed that administration of Ab/PTX LP did not change the neutrophil migration into tumors (Figure S24c). Further analysis showed that 7.5% of intratumoral neutrophils contained liposomes (Figure S24d). Together, the results indicated that Ab/PTX LP was taken up by neutrophils *in vivo* and neutrophils transported liposomes into tumors.

Next, we investigated whether the liposomal formulations could enhance cancer therapy. We i.v. injected Ab/PTX LP to 3LL tumor bearing mice at 5 mg/kg of PTX after laser exposure to tumors or without laser treatment. Interestingly, the combination of administration of Ab/PTX LP and laser exposure to tumors did not inhibit the tumor growth (Figure S24e) and did not improve the mouse survival (Figure S24f). The results (Figure S24c–f) indicated that neutrophil-mediated delivery of PTX-loaded liposomes did not show the therapeutic outcome because liposomes had a low drug content per particle. We also found that mice were tolerant of laser treatment and liposomal formulations (Figure S24g).

To address why neutrophil-mediated delivery of low drug-loaded liposomes did not improve the therapeutic outcome, we studied the particle uptake by neutrophil-like HL-60 cells. We incubated Ab/PTX NC or Ab/PTX LP with the cells at the same concentration of PTX, and then we measured the uptake of PTX. The results showed that the cells took up more PTX when they were incubated with Ab/PTX NC compared to Ab/PTX LP (Figure S25a). We further analyzed the cell uptake efficiencies of PTX (Figure S25b). At the low dose of NPs, the cell uptake efficiency of PTX for Ab/PTX NC was 2 times higher than that of Ab/PTX LP. With the increased dose of NPs, Ab/PTX LP showed a sharp decrease in PTX uptake efficiencies, but Ab/PTX NC showed a gradual decrease. At the high dose of NPs (PTX at 300 μg/mL), the cell uptake efficiency of PTX for Ab/PTX NC was 10 times higher than Ab/PTX LP. The results clearly indicated that the cell uptake efficiencies of PTX for Ab/PTX LP rapidly saturated compared to Ab/PTX NC. This may be associated with the low drug loading in liposomes and the limited cell volume to contain NPs per cell. In the 3LL mouse model, we administered Ab/PTX NC or Ab/PTX LP at the same concentration of PTX to the mice, and then isolated neutrophils in blood to quantify PTX (Figure S25c). We found that the PTX in neutrophils for Ab/PTX NC was 9 times higher than Ab/PTX LP, consistent with the *in vitro* studies on the uptake of PTX (Figure S25a, b). While several studies have shown neutrophil-mediated delivery of low drug-loaded liposomes had the therapeutic benefit,[58] our data clearly show that the high drug loading of drug carriers is essential to design cell-mediated drug delivery including neutrophils.

CONCLUSION

The tumor heterogeneity in tumor types, stages, and patient populations are challenging to develop nanomedicines based on the EPR effect. Blood vasculature is a biological barrier that inhibits the delivery of nanotherapeutics into tumor tissues. Here, we have demonstrated that circulating neutrophils can mediate delivery of NPs across the tumor blood vessel barrier into tumor tissues, and the tumor delivery efficiency is 5% ID/g. Our studies further show that the neutrophil-mediated drug delivery pathway is independent of particle sizes, doses, and material properties (gold NPs, liposomes, and nanocrystals), demonstrating a general drug delivery platform to develop the next generation of cancer nanomedicines by targeting neutrophils. Although photosensitization is used to induce the inflammation response in tumor tissues in our studies, there are many methods available in clinics for neutrophil tumor targeting,[19] such as surgery,[58] radiation therapy,[59] and photodynamic therapy.[60] Therefore, the combination of nanocrystal drugs and neutrophil tumor targeting induced by clinic cancer therapy tools (radiation therapy) may provide opportunities in translating cancer nanomedicines to treat a wide range of cancers.

MATERIALS AND METHODS

Biological and Chemical Agents.

Neutravidin functionalized spherical gold NPs (diameter: 30 and 200 nm) were purchased from Nanopartz (Loveland, CO). Biotin-PEG (5k) (cat. no. MPEG-Biotin-5000–1g) was purchased from Laysan Bio (Arab, AL). Biotin antimouse/human CD11b antibody (Ab, cat. no. 101203), FITC-labeled antimouse CD11b antibody (cat. no. 101205), PE/Cy7-labeled antimouse CD45 antibody (cat. no. 157614), PE/Dazzle 594-labeled antimouse Ly6C antibody (cat. no. 128044), antimouse Ly6G antibody (cat. no. 127649), FITC-labeled antimouse Ly6G antibody (cat. no. 127606), and Alexa Fluor 647-labeled antimouse Ly6G antibody (cat. no. 127610) were obtained from Biolegend (San Diego, CA). Pyropheophorbide-a (Ppa, cat. no. 50–983-032) was purchased from Fisher Scientific (Waltham, MA). Lipopolysaccharide (LPS, cat. no. L2880–100MG, lot no. 039M4004 V) was purchased from Sigma (St. Louis, MO). Paclitaxel (PTX) was provided by Norzer Pharmaceutical (Beijing, China). FITC-PEG-DSPE 5k (cat. no. PLS-9929), Biotin-PEG-DSPE 5k (cat. no. PLS-9953), and mPEG-DSPE 5k (cat. no. PLS-2044) were purchased from Creative PEGWorks (Chapel Hill, NC). Cy3-BSA (cat. no. B3S) was purchased from Protein Mods (Madison, WI).

Cell Lines.

Lewis lung carcinoma (3LL) cells were provided by Dr. Hui Zhang (Department of Pharmaceutical Sciences, Washington State University, Spokane, WA) and glioma 261 (GL261) cells were obtained from Division of Cancer treatments and Diagnostics, National Cancer Institute, NIH. The cells were cultured in a high glucose DMEM medium supplemented with fetal bovine serum (FBS, 10%, v/v), sodium pyruvate (2.5 mM), streptomycin (100 μg/mL) and penicillin (100 U/mL). Human HL-60 cells purchased from ATCC (Manassas, VA, cat. no. CCL-240) were cultured in RPMI1640 with FBS (10%, v/v), streptomycin (100 μg/mL), and penicillin (100 U/mL). All cells were maintained in a humidified 5% CO_2 atmosphere at 37 °C.

Mice.

Wild type C57BL/6 mice (8–10 weeks, 22–24 g) and wild type CD1 mice (5–6 weeks, 22–24 g) were purchased from Jackson Laboratory (Bar Harbor, Maine) and Envigo (Indianapolis, Indiana), respectively. The mice were maintained in polyethylene cages at 20 °C with a 12 h light/dark cycle and were allowed to access food and water *ad libitum*. All animal experiments have been approved by Washington State University IACUC and were performed under anesthesia using intraperitoneal (i.p.) injection of the mixture of ketamine (120 mg/kg) and xylazine (6 mg/kg) in saline.

Photoinduced Acute Inflammation in Tumor Tissues.

The hair on the right back thigh of a C57BL/6 mouse was removed by Nair (Church & Dwight, Ewing, NJ). 2×10^6 3LL cells in 0.1 mL of PBS were then subcutaneously (s.c.) injected to the right back thigh. Tumors were measured every other day by caliper, and the tumor volumes were calculated as $\text{width}^2 \times \text{length}/2$. The light-induced acute inflammation

in tumor tissues was generated when the tumor volume reached 400 mm^3. Mice were anesthetized and retro-orbitally (r.o.) injected with Ppa at 0.6 mg/kg in 0.1 mL PBS containing 5% DMSO (v/v) and 10% Tween 20 (v/v). 0.75 h later, tumors were exposed to 650 nm laser at 150 mW/cm^2 for 2 min. 6, 12, 24, 48, and 72 h after irradiation, blood was collected from the submandibular vein and centrifuged at 800*g* for 10 min to separate blood cells and serum. The blood cells were washed with PBS for 3 times, incubated with PE/Cy7-labeled CD45 antibody and FITC-labeled Ly6G antibody for flow cytometry (FCM, Beckman Coulter, Brea, CA) analysis. Cytokines in serum were measured using IL-6 and TNF-α ELISA MAX Deluxe Sets (Biolegend, San Diego, CA). The CD11b expression levels on circulating leukocytes were studied without laser exposure to tumors or 3 h after laser irradiation. Mice were sacrificed after blood collection. The blood cells were stained by PE/Cy7-labeled CD45 antibody, PE/Dazzle 594-labeled Ly6C antibody, Alexa fluor-647-labeled Ly6G antibody, and FITC-labeled CD11b antibody for flow cytometry. Mouse tumors were isolated, cut into small pieces, and digested for 1 h in 1 mg/mL collagenase type IV in PBS containing 100 μg/mL of DNase I. The cell suspensions were passed through 40 μm cell strainer (Pluriselect, Spring Valley, CA), followed by centrifugation at 800*g* for 10 min to collect single cells. Neutrophil percentages in tumor tissues were analyzed by flow cytometry after incubation with PE/Cy7-labeled CD45 antibody and Alexa fluor-647-labeled Ly6G antibody. Tumor tissues were also lysed using Cell Extraction Buffer (Invitrogen, Eugene, OR) according to the manufacturer's instruction. The supernatants of the lysates were obtained after centrifugation at 20000*g* for 20 min. The concentrations of IL-6 and TNF-α in the supernatants were determined using ELISA MAX Deluxe Sets (Biolegend, San Diego, CA).

Preparation of PEG-Au and Ab-Au NPs.

0.5 mL of Biotin-PEG 5k (at 10 μg/mL, PBS, pH 7.4) or 0.5 mL of Ab (at 100 μg/mL, PBS, pH 7.4) was dropped into 1 mL of neutravidin functionalized spherical gold NPs (at 2 mg/mL, PBS, pH 7.4) under electromagnetic stirring (1000 rpm) at room temperature (RT). The suspension was stirred for 3 h. Then, the PEG-Au NPs and Ab-Au NPs were collected by centrifugation for 30 nm gold NPs at 10000*g* and for 200 nm gold NPs at 1500*g* for 20 min at 4 °C, respectively. The unbound PEG or Ab was removed by resuspension-centrifugation cycles in PBS. The PEG-Au NPs and Ab-Au NPs were kept in PBS at 4 °C. The particle sizes and Zeta potentials were measured in PBS at 25 °C by using Malvern Zetasizer Nano ZS90 (Westborough, MA). The amounts of Ab on Ab-Au NPs were analyzed by SDS-page and quantified by ImageJ software.

Uptake of Gold NPs by Differentiated HL-60 Cells.

Differentiated HL-60 cells were obtained by adding 1.3% DMSO to the medium and culturing for 5 days. The CD11b expression levels were determined by staining the cells with FITC-labeled antimouse CD11b antibody and analyzed by flow cytometry. The differentiated cells were transferred to a six-well plate at 1.5×10^6 cells/well. PEG-Au and Ab-Au (sizes of 30 and 200 nm) were added to each well at dose of 30 μg/mL. The cells were incubated with gold NPs for 45 min and washed with PBS 3 times to remove the unbound NPs. The cell samples were then predigested in 4 mL of concentrated HNO_3 overnight. Two mL of 30% H_2O_2 was added to the samples before heating the samples on

a hot plate at 150 °C. After the samples were diluted to 1 mL and cooled, 1.5 mL of aqua regia was added. The samples were reheated to 150 °C until the volume became 0.5 mL. Afterward, 7.5 mL of mixed acid solution containing 1.5% HNO3 and 1% HCl was added to dilute the samples. The concentrations of gold in the samples were determined by an Agilent 7700 inductively coupled plasma mass spectrometry (ICP-MS, Agilent Technologies, Santa Clara, CA).

Delivery of Gold NPs into Inflamed Tumors.

Tumors were exposed to a laser at 650 nm when the tumor volume reached 400 mm^3. Three hours after the irradiation, PEG-Au NPs or Ab-Au NPs were intravenously (i.v.) injected to mice via a tail vein at different doses (1.2 6, and 30 mg/kg). The mice were sacrificed 24 h after the injection. The tumors and major organs (liver, lung, and spleen) were isolated. The concentrations of gold in tissues were analyzed by ICP-MS after treating the tissue samples with acid, as previously described. To deplete neutrophils, antimouse Ly6G antibody at 10 mg/kg was i.v. injected to mice at 24 h prior to laser irradiation. To determine the gold contents in neutrophils from tumor tissues, tumor tissues were prepared into single cell suspensions as previously described, and neutrophils in tumors were extracted by Pluriselect antimouse-Ly6G S-pluribeads (Pluriselect, Spring Valley, CA). The gold concentrations in neutrophils were analyzed by ICP-MS after the cells were treated with acid.

Preparation of PEG/PTX NC and Ab/PTX NC.

Fifteen mg of PTX in 1.5 mL of chloroform was blown by steady nitrogen gas to form a thin film of PTX crystals. Ten mL of deionized water containing 2 mg of mPEG-DSPE 5k or 2 mg of Biotin-PEG-DSPE 5k was added to the film and sonicated using a tip sonicator (Branson Sonofoer 450) at 10% duty cycle and 20% output for 30 min. Then, the suspension was subjected to a homogenizer (M-110L, Micro-fluidizer) at 18000 psi until the desired particle sizes were achieved. The PEG-coated PTX nanocrystals (PEG/PTX NC) were obtained by centrifugation at 20000g for 25 min. To prepare Ab/PTX NC, 0.2 mg of neutravidin and 0.5 mg of Ab were added to Biotin-PEG/PTX NC suspension and stirred for 2 h at RT. The FITC-labeled PEG/PTX NC and FITC-labeled Ab/PTX NC were prepared by adding 0.5 mg of FITC-PEG-DSPE to the suspension before homogenization. The particle sizes and Zeta potentials were measured in PBS at 25 °C by using Malvern Zetasizer Nano ZS90 (Westborough, MA). To study their morphology, PTX NC, PEG/PTX NC and Ab/PTX NC were vacuum-dried onto a silicon wafer and sputter-coated with a conductive layer of gold palladium (Au/Pd) for 1 min. The samples were imaged by using a scanning electron microscope (SEM, FEI Quanta 200F). The crystalline structure of PEG/PTX NC was characterized by powder X-ray diffraction (PXRD) on a Bruker D8 Venture CPAD diffractometer using graphite monochromatic Cu Ka (λ = 1.54178 Å) radiation. Data sets were collected at a detector distance of 6 cm using 2 Phi scans with 10° increments in 2θ (−20° → −50°). The amounts of Ab on Ab/PTX NC were analyzed by SDS-PAGE and quantified by ImageJ software.

Uptake of PTX NC by Differentiated HL-60 Cells.

2×10^6 differentiated HL-60 cells were incubated with 15 μg/mL FITC-labeled PEG/PTX NC or FITC-labeled Ab/PTX NC at 37 °C for 30 min. The cells were collected by

centrifugation at 400*g* for 5 min and washed with PBS 3 times to remove the unbound NPs. The cell uptake of PTX NC was analyzed by flow cytometry and the cells without NPs treatment were as control. The cells were also centrifuged onto glass slides and stained by DAPI for confocal microscopy.

Neutrophils Transport PTX NC Across Blood Vessel Barrier in Acute Lung Inflammation Model.

CD1 mice were anesthetized and placed in a supine position head up on a board tilted at 15°. Fifteen mg/kg of LPS from *Escherichia coli* in 50 μL of PBS was intratracheally administrated using an FMJ-250 High Pressure Syringe (Penn-Century, Wyndmoor, PA). The mice were kept in a supine position for 2 min after administration to promote LPS delivery to the lung. Four hours after the LPS challenge, FITC-labeled PEG/PTX NC or FITC-labeled Ab/PTX NC at 5 mg/kg were i.v. injected to mice. Four hours later, mice were anesthetized. Bronchoalveolar lavage (BAL) was collected by tracheal intubation and BAL was withdrawn with 3 sequential 0.9 mL of PBS. The BAL was first treated with red blood cell (RBC) lysis buffer for 30 min at room temperature to remove RBC. The amounts of leukocytes were counted on a hemocytometer under a bright field microscope. The cells were incubated with 2.5 μL of Alexa fluor 647-labeled Ly6G antibody for flow cytometry analysis. The cells were also transferred to a coverslip using cytocentrifuge and the cells were fixed with a mounting medium containing DAPI for 1 h before imaging using a confocal microscope (A1R plus, Nikon, Japan).

Uptake of Ab/PTX NC by Leukocytes in Blood.

Three hours after 3LL tumors were exposed to the laser (650 nm) or without laser exposure, mice were i.v. injected with FITC-labeled Ab/PTX NC at 5 mg/kg of PTX. One hour later, blood was collected, and cells were stained with PE/Cy7-labeled CD45 antibody, Alexa fluor-647-labeled Ly6G antibody, and PE/Dazzle 594-labeled Ly6C antibody for flow cytometry analysis. The amount of Ab/PTX NC taken up by different leukocytes was calculated by mean fluorescence intensity of FITC-labeled Ab/PTX NC in cells multiplied with leukocyte percentages in blood and was normalized to that of monocytes when tumor was not exposed to the laser.

Preparation of Ab/PTX LP.

One mg of biotin-PEG-DSPE 5k, 2.5 mg of cholesterol, 6.5 mg of DSPC and 1 mg of PTX were dissolved in 1 mL of chloroform in a round-bottom flask and subjected to rotary evaporation to form a uniform lipid film. Three mL of PBS (pH 7.4) was added, and the lipid film was hydrated under electromagnetic stirring (1000 rpm) at 40 °C for 2 h. The suspension was sonicated by a tip (Branson Sonofoer 450) at 10% duty cycle and 10% output for 1 min. 0.2 mg of neutravidin and 0.5 mg of Ab were added to the suspension, and the mixture was stirred (1000 rpm) at RT for 1 h. The Ab/PTX LP was collected by centrifugation at 20000*g* for 50 min. Free PTX and unbound antibody were removed by twice washing with PBS. The particle sizes and Zeta potentials were measured in PBS at 25 °C using a Malvern Zetasizer Nano ZS90 (Westborough, MA). The PTX loading efficiency was determined by adding acetonitrile to extract PTX from liposomes and analyzed by high performance liquid chromatography (HPLC). The HPLC was performed by a C18 150 ×

4.6 mm column (Restek) in a mobile phase of acetonitrile/deionized water (60/40, v/v) at 1 mL/min at 25 °C. The absorbance was detected at 227 nm.

Neutrophil-Mediated Delivery of PTX-Loaded Liposomes and PTX NC into Tumors.

Three hours after 3LL tumors were exposed to the laser or without laser exposure, mice were i.v. injected with FITC-labeled PTX-loaded liposomes or FITC-labeled PTX NC at 5 mg/kg of PTX. The tumor tissues were isolated 24 h after the injection and the tissues were prepared into single cell suspension using collagenase IV. The cells were analyzed by flow cytometry after staining by PE/Cy7-labeled CD45 antibody and Alexa fluor-647-labeled Ly6G antibody. To image the NPs-laden neutrophils, the tumor tissues were prepared into single cells 6 h after NP injection. The cells were stained by Alexa fluor-647-labeled Ly6G antibody and DAPI for confocal microscopy.

Intravital Microscopy of Neutrophil Mediated Delivery of PTX NC to Tumor Microenvironments.

Acute inflammation in the tumor tissues was generated when the tumor volume reached 400 mm^3. 0.75 h after the laser exposure to tumors at 650 nm, FITC-labeled PEG/PTX NC and Ab/PTX NC at 5 mg/kg were i.v. injected. 0.5 h later, mice were i.v. injected with 5 μg of Alexa fluor 647-labeled Ly6G antibody to mark neutrophils. One h later, 40 μg of Cy3-BSA were r.o. injected to visualize the blood vessels. After the tumor skin was removed to expose tumor tissues under intravital microscope. The images were recorded using confocal microscopy (A1R plus, Nikon, Japan) with a water immersion objective and a resonance scanner (Melville, NY).

In Vivo PTX Distribution.

Ppa at 0.6 mg/kg was ro injected to mice when the tumor volume reached 400 mm^3 under anesthetization. 0.75 h later, tumors were exposed to a 650 nm laser at 150 mW/cm^2 for 2 min. Ab/PTX NC at 7.5 mg/kg were i.v. injected to mice at 3 h after laser irradiation to tumors. Mice were sacrificed at 1, 3, and 6 h after the injection. Liver, spleen, and tumor tissue were isolated, cut into small pieces and homogenized with a Dounce homogenizer. The homogenate was mixed with an equal volume of chloroform for PTX extraction. After centrifugation at 20000*g* for 10 min, the chloroform layer was collected, and the sample was dried. The sample was dissolved in acetonitrile for HPLC analysis.

In Vitro Drug Release.

PEG/PTX NC or Ab/PTX NC containing 0.2 mg of PTX in 1 mL of PBS were sealed in a dialysis bag with the molecular weight cut off at 20 kDa. The dialysis bag was immersed in 50 mL of PBS (pH 7.4). The release was performed by a reciprocating shaker (Incu-shaker IOL, Benchmark, NJ) under 100 rpm at 37 °C. At predetermined time points, a 10 μL suspension from a dialysis bag was withdrawn and mixed with 10 μL of acetonitrile for HPLC analysis.

Drug Release from Differentiated HL-60 Cells.

10^6 number of differentiated HL-60 cells was incubated with 120 μg/mL Ab/PTX NC for cellular uptake for 45 min. The excessive Ab/PTX NC was removed by centrifugation at 400*g* for 3 min. To determine the amounts of Ab/PTX NC internalized by differentiated HL-60 cells, 100 μL chloroform was added to the cells and then the sample was centrifuged at 20000*g* for 10 min. Subsequently, the chloroform layer was collected and dried. Then the sample was dissolved in acetonitrile for HPLC analysis. To determine PTX release from the cells, the cells were cultured in a fresh medium containing 10% FBS. At predetermined time, the medium was withdrawn and centrifuged at 20000*g* for 50 min to obtain the supernatant and the pellet. The supernatant was further centrifuged at 2500*g* using a 30 kDa ultrafiltration tube to obtain free PTX and PTX-protein complexes. Then PTX was extracted by chloroform ready for HPLC analysis.

To investigate the release mechanism of PTX from cells, a liposome loaded with PTX/BSA complexes (PTX/BSA LP) was employed. 0.5 mg of PTX dissolved in 40 μL of ethanol was dropped into 1 mg of BSA dissolved in 3 mL of PBS with stirring (1000 rpm), followed by sonication for 1.5 h to form PTX/BSA complexes. 0.4 mg of biotin-PEG-DSPE 5k, 1 mg of cholesterol, and 2.6 mg of DSPC were dissolved in 1 mL of chloroform in a round-bottom flask and subjected to rotary evaporation to form a uniform lipid film. PTX/BSA complexes were added, and the lipid film was hydrated under electromagnetic stirring (1000 rpm) at 40 °C for 2 h. The suspension was sonicated for 1 min. The PTX/BSA LP was collected by centrifugation at 20000*g* for 50 min. The PTX/BSA LP containing 20 μg of PTX was incubated in 2 mL of PBS or BSA or serum at 37 °C. At predetermined times, the medium was withdrawn and centrifugated at 20000*g* for 50 min. The supernatant was further centrifuged at 2500*g* using a 30 kDa ultrafiltration tube to obtain free PTX and PTX-protein complexes, and PTX was extracted by chloroform and ready for HPLC analysis.

In Vitro Cytotoxicity.

3LL cells were seeded in a 96-well plate at 3000 cells per well and cultured for 24 h. PEG/PTX NC or Ab/PTX NC was added to the 96-well plate at a series of PTX concentrations. The cells were further cultured for 24 or 48 h before adding the MTT solution to a final concentration of 0.5 mg/mL. Four hours later, the culture media were removed. 0.2 mL of DMSO was added and the plates were transferred in a microplate reader (Synergy Neo, BioTek). Ten min later, the absorbance at 570 nm was measured. The cell viability was calculated as (Asample – Ablank)/(Acontrol – Ablank) × 100%, where A_{sample}, A_{control}, and A_{blank} represent the absorbance at 570 nm for the cells treated with PTX formulations, the cells without treatment and the wells without cells, respectively. To simulate the PTX NC release from neutrophils to kill cancer cells, differentiated HL-60 cells containing a series of PTX contents were cultured in fresh medium for 24 or 48 h. The culture medium was transferred to 3LL cells and cultured for 24 or 48 h before the MTT assay. The culture medium from differentiated HL-60 cells without PTX was set as control.

Determination of PTX Loading Efficiency in HL-60 and Neutrophils.

10^6 differentiated HL-60 cells were incubated with Ab/PTX NC or Ab/PTX LP containing the same PTX for 1 h. The incubation was performed at a series of PTX concentrations.

The cells were collected by centrifugation at 400*g* for 3 min and washed with PBS twice to remove the untaken Ab/PTX NC or Ab/PTX LP. 200 μL of chloroform was added to the cells to extract the PTX followed by HPLC analysis. To determine the PTX loading in neutrophil *in vivo*, 10 mg/kg of PTX in Ab/PTX NC or Ab/PTX LP was i.v. injected to 3LL tumor mice at 3 h after laser irradiation. One hour later, blood was collected by heart puncture. Neutrophils were isolated by Pluriselect antimouse-Ly6G S-pluribeads (Pluriselect, Spring Valley, CA) and counted on a hemocytometer. 100 μL of chloroform was added to the cells to extract the PTX followed by HPLC analysis.

In Vivo Therapeutic Efficacy.

To establish the GL261 tumor model, 2×10^6 GL261 cells in 0.1 mL of PBS were then subcutaneously (s.c.) injected to the right back thigh of C57BL/6 mice. Therapeutic studies started when the tumor volume was less than 100 mm^3. To investigate whether neutrophil-mediated delivery of PTX-loaded liposomes improves therapeutic efficiency, 3LL tumor bearing mice were randomly divided into 2 groups and treated with Ab/PTX LP or laser irradiation plus Ab/PTX LP. To investigate the therapeutic efficiency of neutrophil-mediated delivery of PTX NCs, 3LL or GL261 tumor bearing mice were randomly divided into 4 groups and treated with PBS, laser irradiation, Ab/PTX NC, and laser irradiation plus Ab/PTX NC, respectively. the laser at 650 nm irradiated the tumor tissues 0.75 h after r.o. injection with Ppa at 0.6 mg/kg, and the laser power was at 150 mW/cm^2 for 2 min. The drug formulations were administered at 5 mg/kg of PTX 3 h after laser irradiation. The second dose of drug formulations was on Day 6 following the same protocol as the first dose. The mouse tumor volumes and body weights were recorded every 2 days. Mice were euthanized when the tumor volume reached over 2500 mm^3. The H&E staining of major organs in 3LL tumor mice was also performed after two rounds of laser exposure and drug administration.

Statistical Analysis.

Data are expressed as mean ± SD. Statistical analysis was performed by two-tailed Student's *t* test or one-way ANOVA. Statistical significance was indicated as $*P < 0.05$, $**P < 0.01$, or $***P < 0.001$. Significance of survival rates between treatment groups was assessed by log-rank test with 95% CIs using IBM SPSS software (Version 26).

Supplementary Material

Refer to Web version on PubMed Central for supplementary material.

ACKNOWLEDGMENTS

This work was supported by NIH (R01EB027078 and R01GM116823) and NSF (CHE-1827313).

REFERENCES

(1). Hobbs SK; Monsky WL; Yuan F; Roberts WG; Griffith L; Torchilin VP; Jain RK Regulation of transport pathways in tumor vessels: Role of tumor type and microenvironment. P Natl. Acad. Sci. USA 1998, 95 (8), 4607–4612.

(2). Hashizume H; Baluk P; Morikawa S; McLean JW; Thurston G; Roberge S; Jain RK; McDonald DM Openings between defective endothelial cells explain tumor vessel leakiness. Am. J. Pathol. 2000, 156 (4), 1363–1380. [PubMed: 10751361]

(3). Matsumura Y; Maeda H A new concept for macromolecular therapeutics in cancer chemotherapy: mechanism of tumoritropic accumulation of proteins and the antitumor agent smancs. Cancer Res. 1986, 46 (12), 6387–6392. [PubMed: 2946403]

(4). Park K The beginning of the end of the nanomedicine hype. J. Controlled Release 2019, 305, 221–222.

(5). Shi JJ; Kantoff PW; Wooster R; Farokhzad OC Cancer nanomedicine: progress, challenges and opportunities. Nat. Rev. Cancer 2017, 17 (1), 20–37. [PubMed: 27834398]

(6). Park K; Otte A; Park H Perspective on drug delivery in 2050. J. Controlled Release 2022, 344, 157–159.

(7). Chauhan VP; Jain RK Strategies for advancing cancer nanomedicine. Nat. Mater. 2013, 12 (11), 958–962. [PubMed: 24150413]

(8). Hansen AE; Petersen AL; Henriksen JR; Boerresen B; Rasmussen P; Elema DR; af Rosenschold PM; Kristensen AT; Kjaer A; Andresen TL Positron Emission Tomography Based Elucidation of the Enhanced Permeability and Retention Effect in Dogs with Cancer Using Copper-64 Liposomes. ACS Nano 2015, 9 (7), 6985–6995. [PubMed: 26022907]

(9). de Lazaro I; Mooney DJ Obstacles and opportunities in a forward vision for cancer nanomedicine. Nat. Mater. 2021, 20 (11), 1469–1479. [PubMed: 34226688]

(10). Wilhelm S; Tavares AJ; Dai Q; Ohta S; Audet J; Dvorak HF; Chan WCW Analysis of nanoparticle delivery to tumours. Nat. Rev. Mater. 2016, 1 (5), 16014.

(11). Dai Q; Wilhelm S; Ding D; Syed AM; Sindhwani S; Zhang Y; Chen YY; MacMillan P; Chan WCW. Quantifying the Ligand-Coated Nanoparticle Delivery to Cancer Cells in Solid Tumors. ACS Nano 2018, 12 (8), 8423–8435. [PubMed: 30016073]

(12). Sindhwani S; Syed AM; Ngai J; Kingston BR; Maiorino L; Rothschild J; MacMillan P; Zhang Y; Rajesh NU; Hoang T; et al. The entry of nanoparticles into solid tumours. Nat. Mater. 2020, 19 (5), 566–575. [PubMed: 31932672]

(13). Dinarello CA Anti-inflammatory Agents: Present and Future. Cell 2010, 140 (6), 935–950. [PubMed: 20303881]

(14). Nathan C Neutrophils and immunity: challenges and opportunities. Nat. Rev. Immunol 2006, 6 (3), 173–182. [PubMed: 16498448]

(15). Kolaczkowska E; Kubes P Neutrophil recruitment and function in health and inflammation. Nat. Rev. Immunol 2013, 13 (3), 159–175. [PubMed: 23435331]

(16). Vestweber D How leukocytes cross the vascular endothelium. Nat. Rev. Immunol 2015, 15 (11), 692–704. [PubMed: 26471775]

(17). Mayadas TN; Cullere X; Lowell CA The multifaceted functions of neutrophils. Annu. Rev. Pathol 2014, 9, 181–218. [PubMed: 24050624]

(18). Wang Z; Li J; Cho J; Malik AB Prevention of vascular inflammation by nanoparticle targeting of adherent neutrophils. Nat. Nanotechnol 2014, 9 (3), 204–210. [PubMed: 24561355]

(19). Chu D; Dong X; Shi X; Zhang C; Wang Z Neutrophil-Based Drug Delivery Systems. Adv. Mater. 2018, 30 (22), No. e1706245. [PubMed: 29577477]

(20). Chu D; Dong X; Zhao Q; Gu J; Wang Z Photosensitization Priming of Tumor Microenvironments Improves Delivery of Nanotherapeutics via Neutrophil Infiltration. Adv. Mater. 2017, 29 (27), 1701021.

(21). Chu D; Gao J; Wang Z Neutrophil-Mediated Delivery of Therapeutic Nanoparticles across Blood Vessel Barrier for Treatment of Inflammation and Infection. ACS Nano 2015, 9 (12), 11800–11811. [PubMed: 26516654]

(22). Qi J; Jin F; You Y; Du Y; Liu D; Xu X; Wang J; Zhu L; Chen M; Shu G; et al. Synergistic effect of tumor chemo-immunotherapy induced by leukocyte-hitchhiking thermal-sensitive micelles. Nat. Commun. 2021, 12 (1), 4755. [PubMed: 34362890]

(23). Li M; Li S; Zhou H; Tang X; Wu Y; Jiang W; Tian Z; Zhou X; Yang X; Wang Y Chemotaxis-driven delivery of nano-pathogenoids for complete eradication of tumors post-phototherapy. Nat. Commun. 2020, 11 (1), 1126. [PubMed: 32111847]

(24). Gao J; Wang S; Dong X; Wang Z RGD-expressed bacterial membrane-derived nanovesicles enhance cancer therapy via multiple tumorous targeting. Theranostics 2021, 11 (7), 3301–3316. [PubMed: 33537088]

(25). Cabral H; Matsumoto Y; Mizuno K; Chen Q; Murakami M; Kimura M; Terada Y; Kano MR; Miyazono K; Uesaka M; et al. Accumulation of sub-100 nm polymeric micelles in poorly permeable tumours depends on size. Nat. Nanotechnol 2011, 6 (12), 815–823. [PubMed: 22020122]

(26). Zhao ZM; Ukidve A; Kim J; Mitragotri S Targeting Strategies for Tissue-Specific Drug Delivery. Cell 2020, 181 (1), 151–167. [PubMed: 32243788]

(27). Dreher MR; Liu WG; Michelich CR; Dewhirst MW; Yuan F; Chilkoti A Tumor vascular permeability, accumulation, and penetration of macromolecular drug carriers. Jnci-J. Natl. Cancer I 2006, 98 (5), 335–344.

(28). Tong X; Wang ZT; Sun XL; Song JB; Jacobson O; Niu G; Kiesewetter DO; Chen XY Size Dependent Kinetics of Gold Nanorods in EPR Mediated Tumor Delivery. Theranostics 2016, 6 (12), 2039–2051. [PubMed: 27698939]

(29). Perry JL; Reuter KG; Luft JC; Pecot CV; Zamboni W; DeSimone JM Mediating Passive Tumor Accumulation through Particle Size, Tumor Type, and Location. Nano Lett. 2017, 17 (5), 2879–2886. [PubMed: 28287740]

(30). Huo SD; Ma HL; Huang KY; Liu J; Wei T; Jin SB; Zhang JC; He ST; Liang XJ Superior Penetration and Retention Behavior of 50 nm Gold Nanoparticles in Tumors. Cancer Res. 2013, 73 (1), 319–330. [PubMed: 23074284]

(31). Chauhan VP; Stylianopoulos T; Martin JD; Popovic Z; Chen O; Kamoun WS; Bawendi MG; Fukumura D; Jain RK Normalization of tumour blood vessels improves the delivery of nanomedicines in a size-dependent manner. Nat. Nanotechnol 2012, 7 (6), 383–388. [PubMed: 22484912]

(32). Mei H; Cai S; Huang D; Gao H; Cao J; He B Carrier-free nanodrugs with efficient drug delivery and release for cancer therapy: From intrinsic physicochemical properties to external modification. Bioactive materials 2022, 8, 220–240. [PubMed: 34541398]

(33). Junghanns JU; Muller RH Nanocrystal technology, drug delivery and clinical applications. Int. J. Nanomed. 2008, 3 (3), 295–309.

(34). Castano AP; Mroz P; Hamblin MR Photodynamic therapy and anti-tumour immunity. Nat. Rev. Cancer 2006, 6 (7), 535–545. [PubMed: 16794636]

(35). Ohsumi K; Nakagawa R; Fukuda Y; Hatanaka T; Morinaga Y; Nihei Y; Ohishi K; Suga Y; Akiyama Y; Tsuji T Novel combretastatin analogues effective against murine solid tumors: design and structure-activity relationships. Journal of medicinal chemistry 1998, 41 (16), 3022–3032. [PubMed: 9685242]

(36). Yokoi K; Chan D; Kojic M; Milosevic M; Engler D; Matsunami R; Tanei T; Saito Y; Ferrari M; Ziemys A Liposomal doxorubicin extravasation controlled by phenotype-specific transport properties of tumor microenvironment and vascular barrier. J. Controlled Release 2015, 217, 293–299.

(37). Maldiney T; Richard C; Seguin J; Wattier N; Bessodes M; Scherman D Effect of core diameter, surface coating, and PEG chain length on the biodistribution of persistent luminescence nanoparticles in mice. ACS Nano 2011, 5 (2), 854–862. [PubMed: 21291197]

(38). Phillipson M; Kubes P The neutrophil in vascular inflammation. Nat. Med. 2011, 17 (11), 1381–1390. [PubMed: 22064428]

(39). Pillay J; Kamp VM; van Hoffen E; Visser T; Tak T; Lammers JW; Ulfman LH; Leenen LP; Pickkers P; Koenderman L A subset of neutrophils in human systemic inflammation inhibits T cell responses through Mac-1. J. Clin. Invest. 2012, 122 (1), 327–336. [PubMed: 22156198]

(40). O'Hare FM; Watson W; O'Neill A; Grant T; Onwuneme C; Donoghue V; Mooney E; Downey P; Murphy J; Twomey A; et al. Neutrophil and monocyte toll-like receptor 4, CD11b and reactive oxygen intermediates, and neuroimaging outcomes in preterm infants. Pediatric research 2015, 78 (1), 82–90. [PubMed: 25826119]

(41). Lopez-Chaves C; Soto-Alvaredo J; Montes-Bayon M; Bettmer J; Llopis J; Sanchez-Gonzalez C Gold nanoparticles: Distribution, bioaccumulation and toxicity. In vitro and in vivo studies. Nanomed-Nanotechnol 2018, 14 (1), 1–12.

(42). Noireaux J; Grall R; Hullo M; Chevillard S; Oster C; Brun E; Sicard-Roselli C; Loeschner K; Fisicaro P Gold Nanoparticle Uptake in Tumor Cells: Quantification and Size Distribution by sp-ICPMS. Separations 2019, 6 (1), 3.

(43). Du B; Jiang X; Das A; Zhou Q; Yu M; Jin R; Zheng J Glomerular barrier behaves as an atomically precise bandpass filter in a sub-nanometre regime. Nat. Nanotechnol 2017, 12 (11), 1096–1102. [PubMed: 28892099]

(44). Pozzi D; Colapicchioni V; Caracciolo G; Piovesana S; Capriotti AL; Palchetti S; De Grossi S; Riccioli A; Amenitsch H; Lagana A Effect of polyethyleneglycol (PEG) chain length on the bio-nano-interactions between PEGylated lipid nanoparticles and biological fluids: from nanostructure to uptake in cancer cells. Nanoscale 2014, 6 (5), 2782–2792. [PubMed: 24463404]

(45). Wani TU; Raza SN; Khan NA Nanoparticle opsonization: forces involved and protection by long chain polymers. Polym. Bull. 2020, 77 (7), 3865–3889.

(46). Xu J; Gao XP; Ramchandran R; Zhao YY; Vogel SM; Malik AB Nonmuscle myosin light-chain kinase mediates neutrophil transmigration in sepsis-induced lung inflammation by activating beta2 integrins. Nat. Immunol 2008, 9 (8), 880–886. [PubMed: 18587400]

(47). Gao J; Chu D; Wang Z Cell membrane-formed nanovesicles for disease-targeted delivery. J. Controlled Release 2016, 224, 208–216.

(48). Kulkarni TA; Bade AN; Sillman B; Shetty BLD; Wojtkiewicz MS; Gautam N; Hilaire JR; Sravanam S; Szlachetka A; Lamberty BG; et al. A year-long extended release nanoformulated cabotegravir prodrug. Nat. Mater. 2020, 19 (8), 910. [PubMed: 32341511]

(49). Zhao R; Hollis CP; Zhang H; Sun L; Gemeinhart RA; Li T Hybrid nanocrystals: achieving concurrent therapeutic and bioimaging functionalities toward solid tumors. Mol. Pharmaceutics 2011, 8 (5), 1985–1991.

(50). Reutershan J; Basit A; Galkina EV; Ley K Sequential recruitment of neutrophils into lung and bronchoalveolar lavage fluid in LPS-induced acute lung injury. Am. J. Physiol-Lung C 2005, 289 (5), L807–L815.

(51). Matthay MA; Zemans RL; Zimmerman GA; Arabi YM; Beitler JR; Mercat A; Herridge M; Randolph AG; Calfee CS Acute respiratory distress syndrome. Nat. Rev. Dis Primers 2019, 5 (1), 18. [PubMed: 30872586]

(52). Jarvis M; Krishnan V; Mitragotri S Nanocrystals: A perspective on translational research and clinical studies. Bioeng Transl Med. 2019, 4 (1), 5–16. [PubMed: 30680314]

(53). Paal K; Muller J; Hegedus L High affinity binding of paclitaxel to human serum albumin. Eur. J. Biochem. 2001, 268 (7), 2187–2191. [PubMed: 11277943]

(54). Abdollah MRA; Carter TJ; Jones C; Kalber TL; Rajkumar V; Tolner B; Gruettner C; Zaw-Thin M; Baguna Torres J; Ellis M; et al. Fucoidan Prolongs the Circulation Time of Dextran-Coated Iron Oxide Nanoparticles. ACS Nano 2018, 12 (2), 1156–1169. [PubMed: 29341587]

(55). Xu HZ; Li TF; Ma Y; Li K; Zhang Q; Xu YH; Zhang YC; Zhao L; Chen X Targeted photodynamic therapy of glioblastoma mediated by platelets with photo-controlled release property. Biomaterials 2022, 290, No. 121833. [PubMed: 36201945]

(56). Chen MH; Liu TY; Chen YC; Chen MH Combining Augmented Radiotherapy and Immunotherapy through a Nano-Gold and Bacterial Outer-Membrane Vesicle Complex for the Treatment of Glioblastoma. Nanomaterials 2021, 11 (7), 1661. [PubMed: 34202555]

(57). Shen S; Wu Y; Liu Y; Wu D High drug-loading nanomedicines: progress, current status, and prospects. Int. J. Nanomedicine 2017, 12, 4085–4109. [PubMed: 28615938]

(58). Xue JW; Zhao ZK; Zhang L; Xue LJ; Shen SY; Wen YJ; Wei ZY; Wang L; Kong LY; Sun HB; et al. Neutrophil-mediated anticancer drug delivery for suppression of postoperative malignant glioma recurrence. Nat. Nanotechnol 2017, 12 (7), 692. [PubMed: 28650441]

(59). Takeshima T; Pop LM; Laine A; Iyengar P; Vitetta ES; Hannan R Key role for neutrophils in radiation-induced antitumor immune responses: Potentiation with G-CSF. Proc. Natl. Acad. Sci. U. S. A. 2016, 113 (40), 11300–11305. [PubMed: 27651484]

(60). Kousis PC; Henderson BW; Maier PG; Gollnick SO Photodynamic therapy enhancement of antitumor immunity is regulated by neutrophils. Cancer Res. 2007, 67 (21), 10501–10510. [PubMed: 17974994]

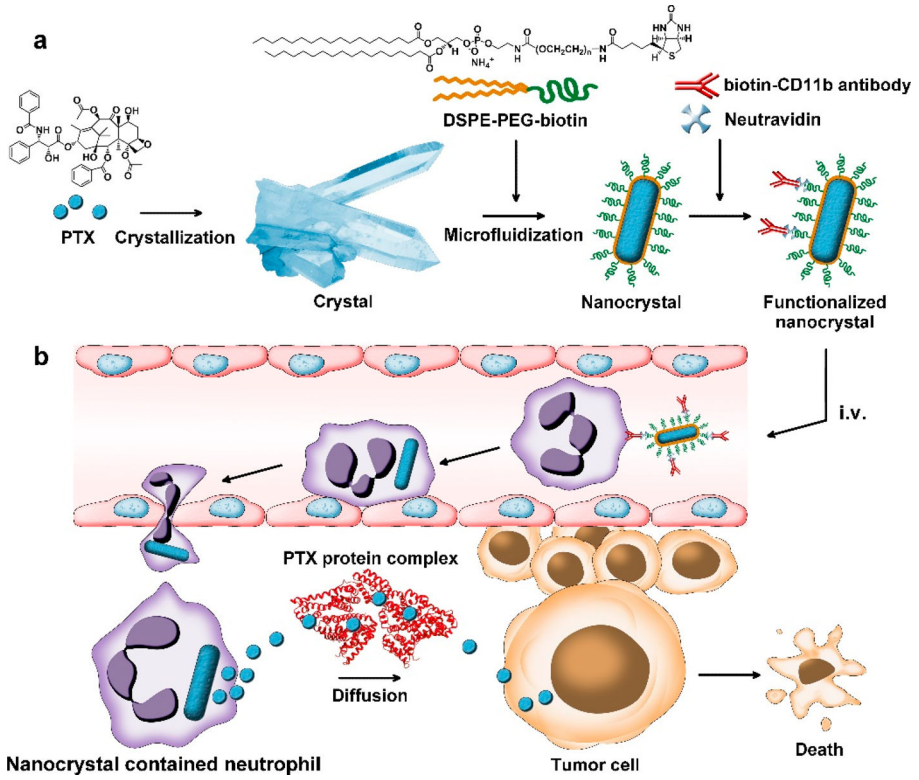

Figure 1.

Design of nanocrystal drugs (paclitaxel nanocrystals, PTX NC) for targeting activated neutrophils in blood to enhance cancer therapies. (a) Preparation process of Ab/PTX NC including production of nanocrystals and bioconjugation of anti-CD11b for neutrophil targeting. (b) Neutrophil-mediated delivery of Ab/PTX NC into tumor microenvironments. After Ab/PTX NC are intravenously administered to a tumor bearing mouse, they are specifically taken up by activated neutrophils in blood, and subsequently, the neutrophils transport Ab/PTX NC across tumor vasculature. PTX releases from PTX NC in neutrophils and binds to proteins to form a PTX-protein complex for the sustainable killing of tumor cells.

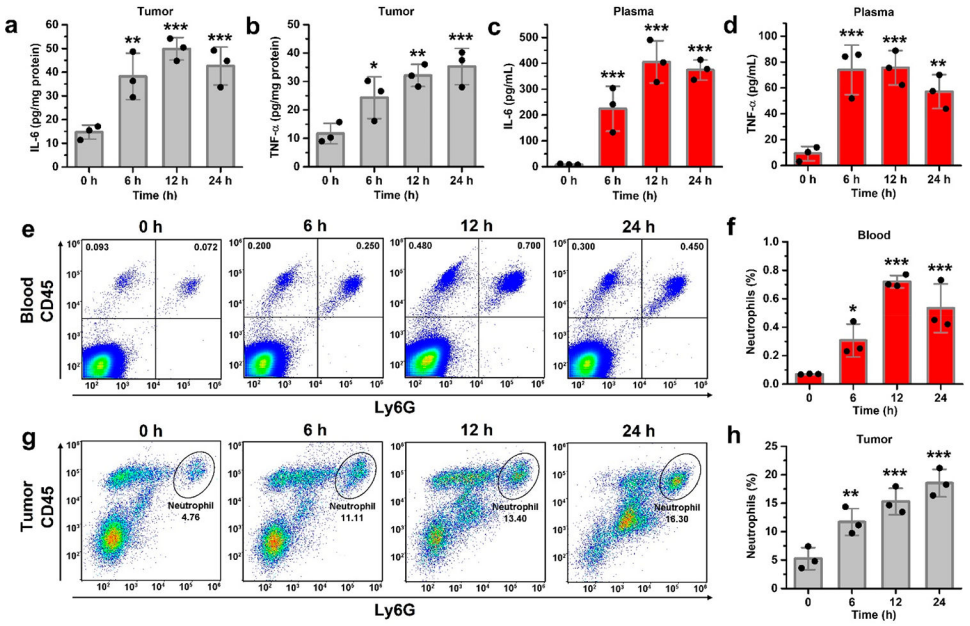

Figure 2.

Laser irradiation induces an acute inflammation response in tumor microenvironments. Laser exposure to tumor tissues produced (a) IL-6 and (b) TNF-α in tumor tissues, as well as (c) IL-6 and (d) TNF-α in plasma determined by ELISA. (e) Dynamics of neutrophils in blood analyzed by flow cytometry after laser irradiation and (f) their quantification. (g) Dynamics of neutrophils in tumor tissues analyzed by flow cytometry after laser irradiation and (h) their quantification. Neutrophils were marked with anti-CD45 antibody and anti-Ly6G antibody. The data are expressed as mean ± SD ($n = 3$). Statistical analysis compared with controls (at 0 h). *$P < 0.05$, **$P < 0.01$, and ***$P < 0.001$.

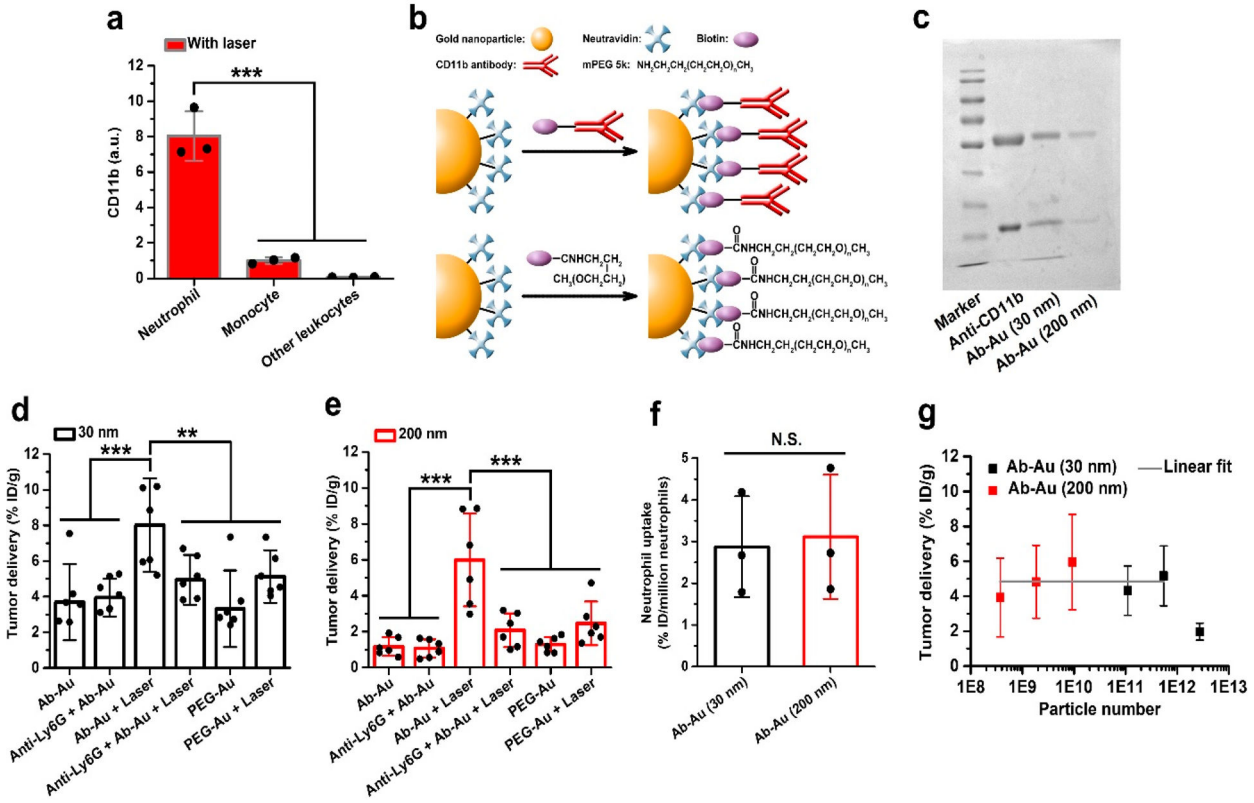

Figure 3.

Neutrophil-mediated delivery of NPs into tumors is independent of particle size and their dose. (a) CD11b expression levels of leukocytes in blood at 3 h after 650 nm laser irradiation of mouse tumor tissues. Neutrophils were marked by $CD45^+/Ly6G^+/Ly6C^{low}$, monocytes were marked by $CD45^+/LyC6^+/Ly6G^-$, and other leukocytes were marked by $C45^+/Ly6G^-/Ly6C^-$. The CD11b expression levels were calculated as multiplying the cell percentages and mean fluorescence intensities of CD11b determined by flow cytometry and were normalized to that of monocytes. (b) Scheme for preparation of PEG-Au NPs or Ab-Au NPs. PEG or Ab was coated onto NPs through the binding between biotin and neutravidin. (c) SDS-PAGE analysis of Ab on gold NPs. Tumor NP delivery efficiencies of (d) 30 nm NPs and (e) 200 nm NPs. Neutrophil depletion was performed using 10 mg/kg of anti-Ly6G antibody injected 24 h before laser irradiation (Ly6G + Ab-Au + laser) or without laser irradiation (Ly6G + Ab-Au). PEG-Au NPs were used as the control. (f) Percentages of the injected dose of gold NPs per million neutrophils isolated from inflamed tumor tissues. The administered doses were 1.2 mg/kg for 30 nm NPs and 6 mg/kg for 200 nm NPs in (d), (e), and (f). (g) Neutrophil-mediated tumor delivery of Ab-Au NPs in a wide range of injected doses of NPs. This was calculated by the percentages of injected dose in tumors under laser irradiation, subtracting those without laser irradiation. The administered doses of 30 nm NPs and 200 nm were 1.2, 6, and 30 mg/kg, respectively. Quantitative data are expressed as the mean ± SD ($n = 3$ in a and f, $n = 6$ in d, e, and g). $^{**}P < 0.01$ and $^{***}P < 0.001$.

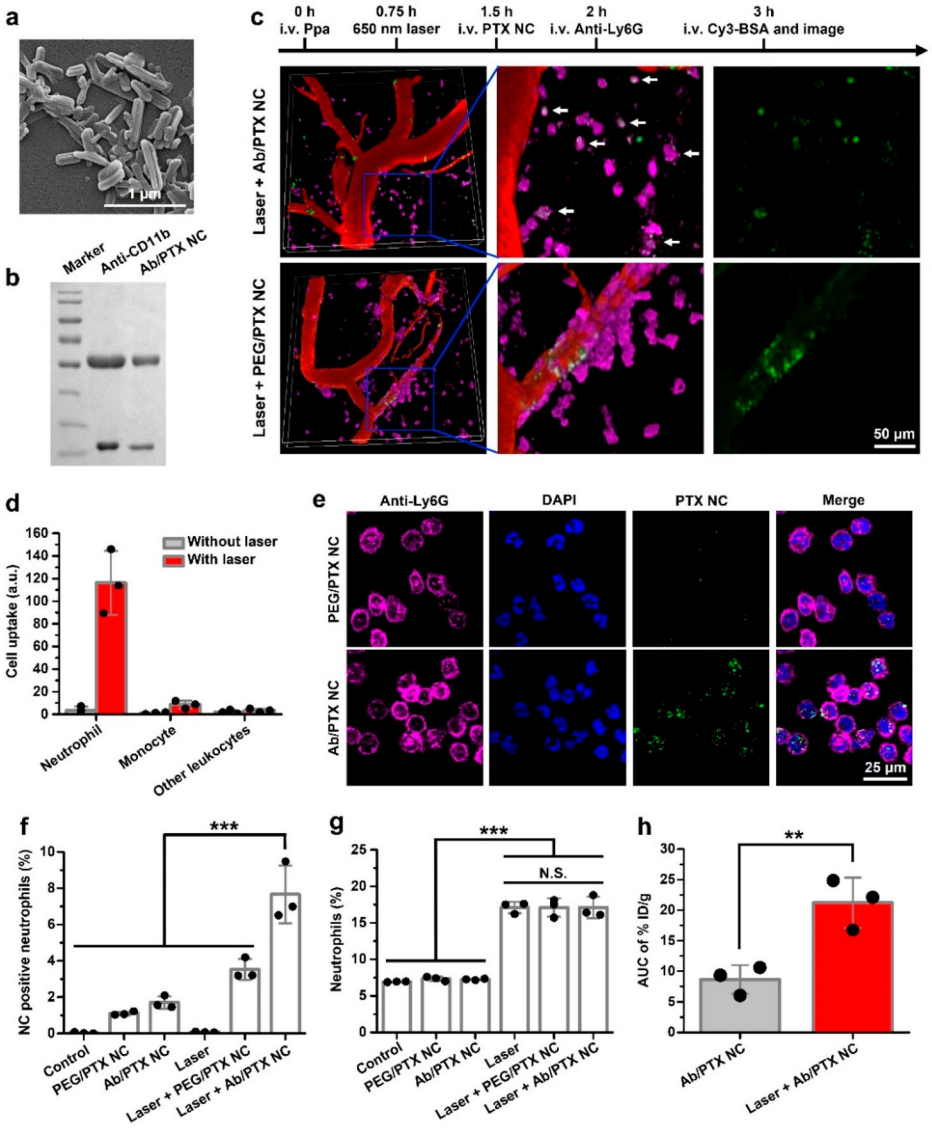

Figure 4.

Neutrophil-mediated delivery of Ab/PTX NC into tumor microenvironments. (a) SEM images of the Ab/PTX NC. (b) SDS-PAGE analysis of Ab on Ab/PTX NC. (c) Intravital images of tumors show that neutrophils transport Ab/PTX NC across tumor vasculature. The imaging protocol is shown above (c). After laser was exposed to tumor tissues, 5 mg/kg FITC labeled PEG/PTX NC or Ab/PTX NC (green) were i.v. administered. Neutrophils were stained by Alexa fluor 647 antimouse Ly6G antibody (violet), and blood vessels were visualized by Cy3-BSA (red). (d) Neutrophils are major leukocytes to take up Ab/PTX NC after laser exposure to tumors. The analysis was based on fluorescent intensity of Ab/PTX NC, and percentages of leukocytes determined by flow cytometry (Figure S14). The flow cytometry was performed 1 h after i.v. injection of Ab/PTX NC. Circulating leukocytes were stained by anti-CD45 antibody. Neutrophils and monocytes were identified as $Ly6G^{+}/Ly6C^{low}$ and $Ly6G^{-}/Ly6C^{+}$ populations, respectively. (e) Confocal microscopy images of neutrophils isolated from tumors at 6 h after i.v. injection of nanocrystals. (f)

Percentages of neutrophil containing nanocrystals among the total cells and (g) percentages of total neutrophils in tumors 24 h after administration of nanocrystals. (h) 6 h PTX tumor accumulation (area under the curve (AUC)) after i.v. administration of Ab/PTX NC at 7.5 mg/kg of PTX. PTX concentrations were determined by HPLC. The data are expressed as mean ± SD ($n = 3$). $^{**}P < 0.01$ and $^{***}P < 0.001$.

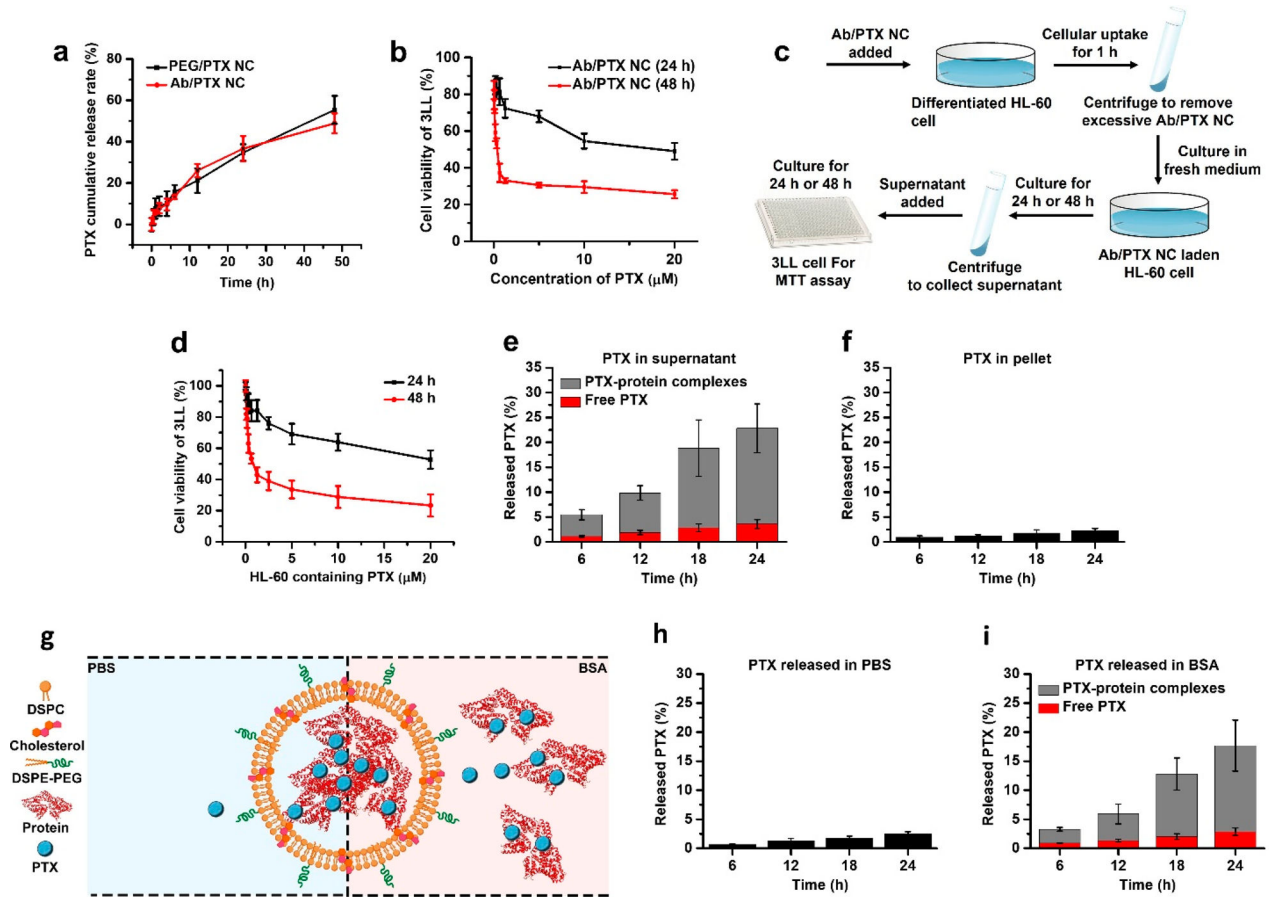

Figure 5.

PTX NC sustains the release from neutrophils via PTX-protein complexes to kill cancer cells. (a) Release profiles of PTX in the formulations of PEG/PTX NC and Ab/PTX NC in PBS (pH 7.4) at 37 °C. (b) Cell viability of 3LL cells treated with Ab/PTX NC after 24 and 48 h. (c) Experimental design to address the delivery of PTX from neutrophil-like cells (differentiated HL-60 cells) containing PTX NC to tumor cells *in vitro*. (d) Cell viability of 3LL cells after they were cultured with the culture medium of neutrophil-like cells containing PTX NC following the experiment as shown in (c). PTX contents in the supernatant (e) and pellet (f) of the culture medium of neutrophil-like cells containing PTX NC. The supernatant was centrifuged using a 30 kDa ultrafilter to obtain free PTX and PTX-protein complexes. (g) Schematic diagram of PTX release from PTX/BSA LP. The time courses of PTX release from PTX/BSA LP in PBS (h) or PBS containing BSA (i). Data are expressed as mean ± SD ($n = 3$).

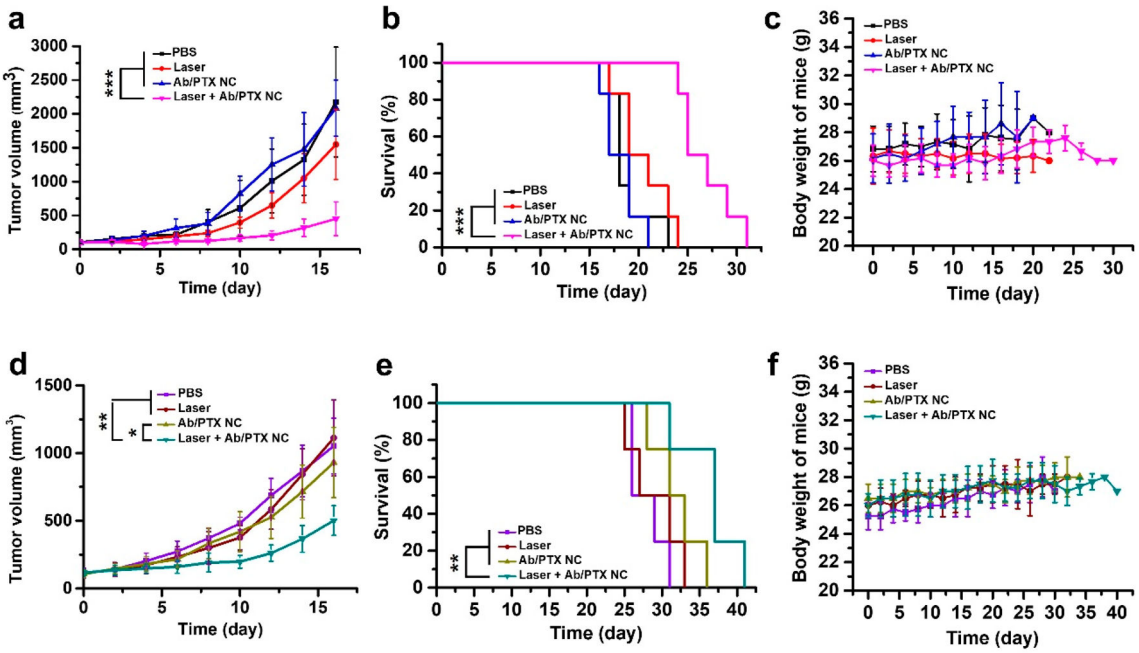

Figure 6.

Neutrophil-mediated delivery of PTX NCs enhances mouse survival in cancer. (a) The mouse tumor growth, (b) the mouse survival, and (c) the mouse body weight in a 3LL tumor mouse model after mice were treated with several PTX formulations and laser exposure to tumors. (d) The mouse tumor growth, (e) the mouse survival, and (f) the mouse body weight in a GL261 tumor mouse model after mice were treated with several PTX formulations and laser exposure to tumors. The treatments started when the tumor volume reached 100 mm^3. All formulations containing a dose of PTX at 5 mg/kg were i.v. injected on day 0 and day 6. Data are expressed as mean ± SD ($n = 6$ in a, b, and c, $n = 4$ in d, e, and f). *$P < 0.05$, ***$P < 0.01$ and ***$P < 0.001$.